Cite This: Nano Lett. 2017, 17, 6961-6967

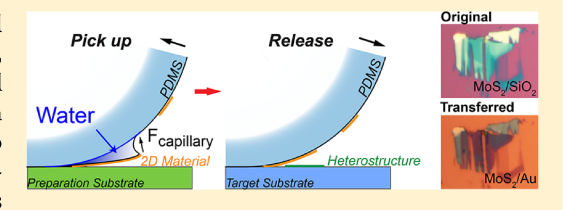
Capillary-Force-Assisted Clean-Stamp Transfer of Two-Dimensional **Materials**

Xuezhi Ma, † Qiushi Liu, † Da Xu, † Yangzhi Zhu, ‡ Sanggon Kim, ‡ Yongtao Cui, § Lanlan Zhong, ¶ and Ming Liu*, † , ∥ [o

[†]Department of Electrical and Computer Engineering, [‡]Department of Chemical and Environmental Engineering, [§]Department of Physics, and Material Science and Engineering Program, Bourns College of Engineering, University of California, Riverside, California 92521, United States

Supporting Information

ABSTRACT: A simple and clean method of transferring two-dimensional (2D) materials plays a critical role in the fabrication of 2D electronics, particularly the heterostructure devices based on the artificial vertical stacking of various 2D crystals. Currently, clean transfer techniques rely on sacrificial layers or bulky crystal flakes (e.g., hexagonal boron nitride) to pick up the 2D materials. Here, we develop a capillary-force-assisted cleanstamp technique that uses a thin layer of evaporative liquid (e.g., water) as



an instant glue to increase the adhesion energy between 2D crystals and polydimethylsiloxane (PDMS) for the pick-up step. After the liquid evaporates, the adhesion energy decreases, and the 2D crystal can be released. The thin liquid layer is condensed to the PDMS surface from its vapor phase, which ensures the low contamination level on the 2D materials and largely remains their chemical and electrical properties. Using this method, we prepared graphene-based transistors with low charge-neutral concentration $(3 \times 10^{10} \text{ cm}^{-2})$ and high carrier mobility (up to 48 820 cm² V⁻¹ s⁻¹ at room temperature) and heterostructure optoelectronics with high operation speed. Finally, a capillary-force model is developed to explain the experiment.

KEYWORDS: 2D materials, stamp transfer, capillary force, heterostructure

wo-dimensional (2D) materials, such as graphene and transition metal dichalcogenides (TMDC), have stimulated extensive research efforts in the fields of nanoelectronics and optoelectronics due to their exceptional electrical and optical properties.^{1,2} By stacking different 2D material layers in van der Waals (vdW) heterostructures, new device concepts with outstanding functionalities have been demonstrated.³⁻⁶ Both the full exploration of 2D material properties and the fabrication of heterostructures require a clean and intact transfer technique to move these layered materials from the preparation substrates onto target positions without compromising their properties or qualities, and in particular, without any contamination. So far, poly(methyl methacrylate) (PMMA) has been widely used as the holder for transferring, owing to the simple yet versatile procedure. However, PMMA always leaves a thin layer of long-chain molecules on the 2D material surfaces, even after exhaustive rinsing with various organic solvents.8 This residual contaminates the sample surfaces and has become a major limiting factor restricting the device performance. To solve this problem, sacrificial layers, such as a thin metal^{9,10} or polylactic acid (PLLA) film, ¹¹ have been used to separate PMMA from the 2D materials. However, it introduces extra fabrication steps including deposition, dissolving, and washing, which are tedious in particular in the preparation of heterostructures. Polydimethylsiloxane (PDMS)based stamp transfer method has been exploited as a drytransfer technique for nanoelectronics. 12,13 So far, it cannot peel off 2D monolayers directly from silicon dioxide (SiO₂)

substrate because the adhesion energy between PDMS and 2D monolayers (\sim 7 mJ/m² for graphene)¹⁴ is far weaker than the vdW energy between 2D materials and SiO₂ (~240 mJ/m² for graphene). To increase the bonding energy between the dry-transfer stamp and 2D monolayers, atomically flat surfaces of hexagonal boron nitride (h-BN) flakes have been recently introduced. 16-18 As a trade-off, removing this BN layer to expose the functional 2D materials is challenging.

In this paper, we report a simple and universal capillaryforce-assisted clean-stamp method to transfer 2D materials. We demonstrate the flexibility and quality of this approach for single- and multi-layer materials by the fabrication and characterization of a graphene-based field effect transistor (Gr-FET) and a vertically stacked heterostructure photodetector. The key concept of this technique is the utilization of a thin liquid film between a PDMS stamp and 2D monolayers as a dynamic bonding enhancer. The thin liquid film acts as an instant glue between the PDMS stamp and 2D materials and subsequently peels them off from the substrates. After the thin liquid layer evaporates, the capillary force vanishes and leaves the 2D monolayers ready to be released onto new substrates. The transient adhesion-enhancing mechanism bypasses the trade-off between the peeling-off step and the releasing step, in which the increase in adhesion fosters the peeling-off but

Received: August 12, 2017 Revised: October 16, 2017 Published: October 23, 2017

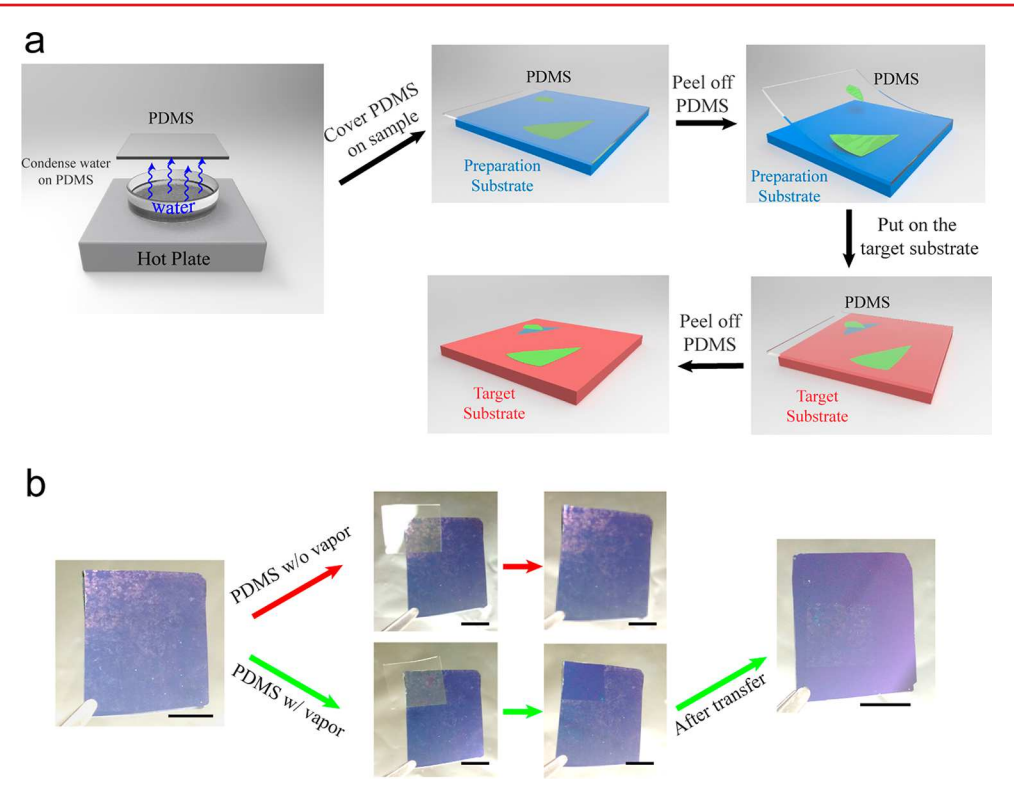


Figure 1. (a) Schematic diagram of the capillary-force-assisted transfer procedure. (b) The comparison between the adhesion capability of a dry PDMS film and a wet PDMS film. The dry one cannot peel off any MoS₂ flakes from the SiO₂ substrate (upper row, red path), while a wet PDMS film can pick up all flakes (lower row, green path). The picked-up flakes can be transferred to the target substrate (right). All scale bars are 1 cm. A standard PMMA-assisted method can be found in the Supporting Information for comparison.

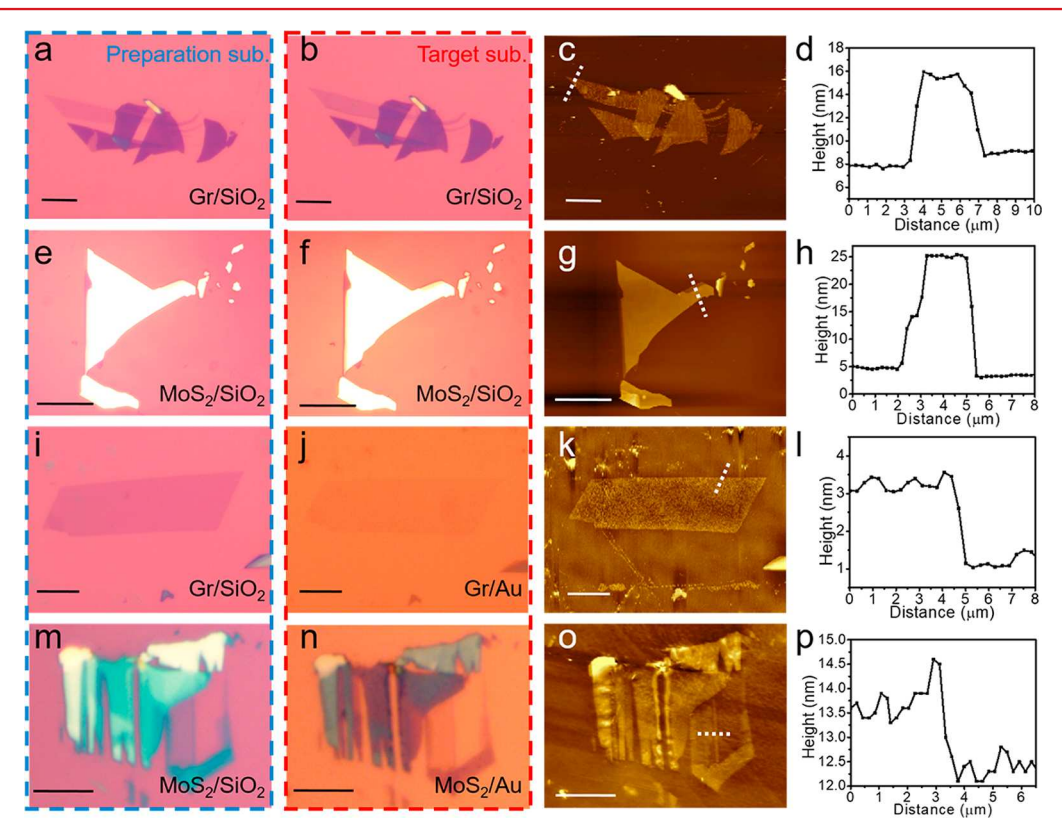


Figure 2. Optical microscope images and AFM cross-section images of graphene and MoS_2 flakes transferred from the preparation substrates (300 nm SiO_2/Si , labeled as SiO_2) to the target substrates (300 nm SiO_2/Si and super-flat gold substrates). All scale bars are 10 μ m.

hinders the releasing step. 19 Because this method uses a distilled volatile liquid film instead of a solid sacrificial layer, both physical damage and chemical contamination are minimized in this process. In addition, the 2D monolayers can be released to a target area on the receiving substrate by aligning the PDMS stamp under an optical microscope because they can be located optically or with the help of a marker. Using this method, we fabricated a Gr-FET by the direct transfer of an exfoliated graphene monolayer onto palladium-gold electrodes, which demonstrated a near-zero charge-neutral voltage and a high electron mobility of ~48,820 cm² V⁻¹ s⁻¹ under room temperature, indicating ultralow surface doping and defect level incorporated from the transfer process. It is worth noting that this mobility level is the highest for graphene monolayers on SiO₂ surfaces, several times higher than those achieved by PMMA-based wet transfer with low-residue sacrificial layers, the previous best performers on SiO₂.²⁰ We also demonstrate the versatility of this quick and clean transfer technique in the fabrication of high-performance 2D heterostructure devices and have achieved fast optical response with a graphene/MoS₂/ graphene heterostructure photodetector. A capillary force model is discussed for the revealing of the role of liquid in this technique.

The capillary-force-assisted clean transfer process is illustrated in Figure 1. A thin PDMS film is first held over a beaker with boiling deionized (DI) water (or other solvents) for 3-5 s to condense water on the PDMS surface. The PDMS is then quickly yet gently placed on the substrate with 2D monolayers, which are prepared by the mechanical exfoliation method and confirmed by Raman spectroscopy. After forming a conformal contact with the SiO₂ substrate, the PDMS is quickly peeled off, starting from one side and maintaining a small angle between the PDMS and the substrate during the process. Firmly pulled by the capillary force, the 2D monolayers now adhere to the PDMS and are ready to be transferred onto the target substrate. Under an optical microscope, the PDMS stamp is aligned to the target substrate using a translation stage so that the transferred 2D monolayers precisely overlap with the target region on the substrate. A simple pressing step will release the 2D monolayers. Because the soft PDMS is gently placed on the substrate, this releasing process will not damage the existing surface structures on the target substrate, such as microelectrodes and other 2D monolayers. By the simple repetition of this transfer process, 2D heterostructures can be built layer-

To show the determining role of the capillary force in this new method, we compare the effectiveness of transferring MoS₂ flakes by dry and vapor-wet PDMS stamps in Figure 1b. The dry PDMS stamp can hardly pick up any MoS₂ flake from the substrate (Figure 1b, red path), whereas the vapor-wet PDMS stamp was able to transfer all flakes underneath to a clean SiO₂/Si substrate (Figure 1b, green path). It is also worth noting that this quick and easy process requires minimal instrumentation and time (Video S1). Moreover, in the case in which the target material is sensitive to water, other volatile liquids can be used (e.g., ethanol has been tried to transfer graphene in Figure S3)

Figure 2 shows the optical microscope images and atomic force microscopy (AFM) characterization of the transferred results. Large-area graphene flakes containing both single and multilayer regions were transferred with high fidelity from a 300 nm-SiO $_2$ /Si substrate (Figure 2a) to another SiO $_2$ /Si substrate (Figure 2b). The AFM image (Figure 2c) shows that both monolayer and multilayer regions of the graphene flake are

wrinkle- and crack-free after the transfer. The low roughness of the flake surface indicates that it is clean of any particle or organic residues. Owing to the low adhesion energy on a dry PDMS, the graphene flakes can also be released to other types of substrate, such as a freshly peeled ultraflat gold substrate (Figure 2i–k; surface roughness of 0.6 nm), prepared by the fabrication method introduced elsewhere. This transfer technique can be applied not only to hydrophilic materials like graphene but also to hydrophobic materials, such as molybdenum disulfide (MoS₂). Figure 2e,m shows the optical microscope images of MoS₂ flakes transferred to a 300 nm SiO₂/Si substrate and a gold substrate with high fidelity, respectively.

A three-terminal back-gated Gr-FET was fabricated to characterize the electrical properties of graphene monolayers prepared by this method. The device layout is shown in Figure 3a. It was prepared by transferring a graphene monolayer

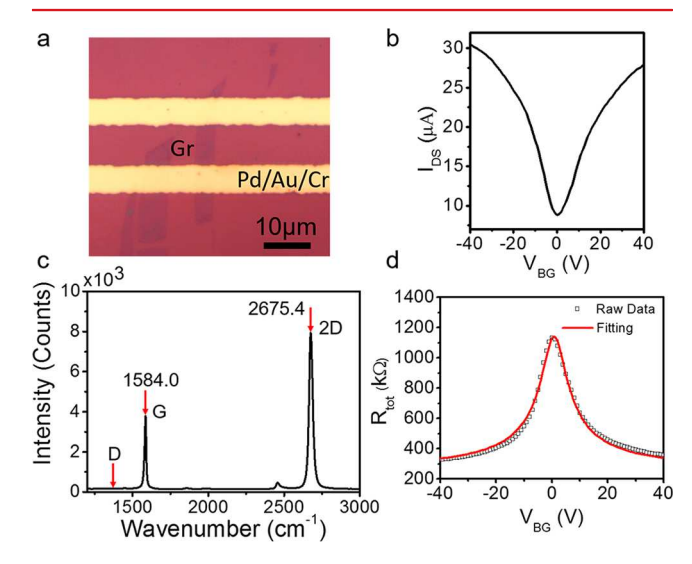


Figure 3. Electrical and Raman characteristic of a graphene FET prepared by direct transferring of a graphene monolayer onto electrodes. (a) The optical microscope image of the device layout. The electrode contains 10 nm Pd, 80 nm Au, and 3 nm Cr. (b) Source-drain current of the Gr-FET vs the back-gate bias $V_{\rm BG}$, measured under ambient conditions at room temperature. The thickness of the SiO₂ gate oxide is 300 nm. $V_{\rm DS}$ is 10 mV. The charge-neutral-point gate voltage is 0.45 V. (c) Raman spectrum of the graphene channel region. (d) The total resistance $R_{\rm tot}$ vs $V_{\rm BG}$ with both the experimental data (squares) and the modeling result (line).

directly onto prepatterned electrodes (10, 80, and 3 nm for Pd, Au, and Cr, respectively, from top to bottom), which were defined by standard photolithography and metal deposition. This fabrication process avoids the direct contact of the graphene monolayer with any polymer solution, such as PMMA or photoresist, and thus minimizes the contamination from polymer residuals. The quality of the transferred graphene was confirmed by Raman spectroscopy. As shown in Figure 3c, the spectrum features a symmetric Lorentzian-shaped G band centered at 1584.0 cm⁻¹ and a 2D band at 2675.4 cm⁻¹, with narrow peak widths at full width at half-maximums (fwhms) of 11.6 and 27.6 cm⁻¹, respectively. The absence of the D' band at 1620 cm⁻¹ indicates a low density of random impurities or surface charges. This is also evidenced in the undetectable D band, which is caused by the disorders in sp² hybridized carbon system. The average intensity ratio of the 2D to G is larger than

2, further confirming the high quality of the monolayer graphene. No PMDS peak (~1410 cm⁻¹) shows up in the spectrum. All of these Raman characterization results are in good consistency with the high-quality monolayer graphene reported in the literature.

The cleanliness of the transferred graphene monolayer is also evidenced in the current—voltage characteristic of the Gr-FET device. Figure 3b shows the room-temperature conductivity as a function of the back-gate voltage ($V_{\rm BG}$) of the device. The $V_{\rm BG}$ for the charge-neutral point (CNP) is very close to zero ($V_{\rm BG,CNP}=0.45~\rm V$ with 300 nm SiO₂ as gate oxide) in the asprepared device, revealing a charge-neutral doping level ($n_{\rm CN}$) of $\sim 3 \times 10^{10}~\rm cm^{-2}$, where $n_{\rm CN}=\alpha V_{\rm BG,CNP}$, with $\alpha=7.2\times 10^{10}~\rm cm^{-2}~\rm V^{-1}$ derived from a parallel-plate capacitor model. The carrier mobility of the device can be extracted from a device model with the contact resistance and considered. The mobility is found to be $\sim 48~820~\rm cm^2~\rm V^{-1}~s^{-1}$ at room temperature. (Details are listed in the Supporting Information.)

Due to the simplicity of the transfer procedure, the exceptional cleanness of the sample surface, and the capability for repeated stacking of various 2D monolayers, this technique can also be used to prepare high-performance vertically stacked vdW heterostructures. Heterostructure devices have been demonstrated for several applications, including graphene stacked on h-BN for high-mobility FETs,²⁴ tunneling field effect transistors (TFETs), and photodetectors.^{25,26} Previous demonstrations of heterostructure applications mainly rely on PMMA-assisted transfer,²⁴ in which the complete removal of polymer residues is challenging, or h-BN-assisted hot-pickup technique in which the exposure of 2D materials to electrodes or environments is difficult. The capillary-force-assisted transfer demonstrated here is a quick and convenient method to build them.

As a proof-of-concept, graphene/MoS₂/graphene (Gr/ MoS₂/Gr) vdW heterostructure devices (Figure 4a) were fabricated and characterized. The active regions were prepared by the successive transfers of a single-layer graphene film (yellow outlined area in Figure 4b), a 6 nm thick MoS₂ flake (green color region), and another single-layer graphene film (blue outlined area) from their original substrates onto prepatterned electrodes. The positions of the transferred 2D flakes are carefully adjusted through a translation stage during each film transfer to ensure a large Gr/MoS₂/Gr sandwich area (the overlap of the blue and yellow outlined areas). In this region, the photon-generated electron-hole pairs in the MoS₂ layer can be separated and collected by the top and the bottom graphene electrodes (Gr_T and Gr_B) according to two driving mechanisms. One is the force from the external electric field applied between Gr_T and Gr_B, and the other is from the built-in electric field created by the asymmetric band structures. Figure 4c shows the photocurrent as a function of time measured under the alternating 532 nm laser illumination (spot size of ~1 μ m) at four different optical powers (45, 90, 160, and 225 μ W). The photocurrents have fast temporal responses at both the rising edges (from off to on) and the falling edges (from on to off), and are stable at the "on" states over long-term (\sim 60 s) measurements. Such a clear switching steps and the stable ON current indicate the absence of trapped states at the interfaces, which usually leads to a gradual change of photocurrent due to the slow charge transfer process. The fast photoresponse leads to the high operation speed as a photodetector. To characterize its high-speed performance (Figure 4d), we used a mechanical chopper to modulate the laser beam from 1 k to 10 kHz and

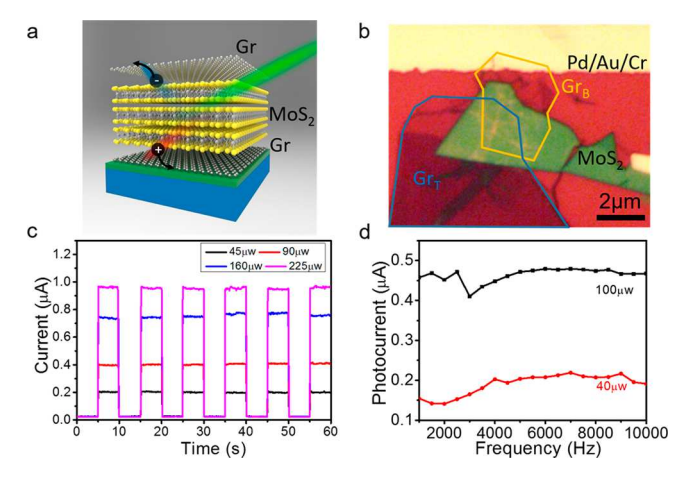


Figure 4. Photocurrent generation in a vertically stacked graphene— ${\rm MoS_2-graphene}$ heterostructure. (a) The schematic illustration of the heterostructure device layout. (b) An optical microscope image of the device, prepared by successive transferring of a monolayer graphene bottom electrode (yellow-outlined region), a few-layer ${\rm MoS_2}$ flake, and a graphene top electrode (blue-outlined region) onto the electrode. (c) The photocurrent measurement of the sandwiched region (intersection of the blue- and yellow-outlined regions), excited by a 532 nm laser with various powers. The characterizations were performed under ambient conditions, with both the bias voltage $(V_{\rm DS})$ and the back-gate voltage $(V_{\rm BG})$ set as zero. (d) The frequency-dependent photocurrent measurement.

used a lock-in amplifier (Stanford Research Systems, SR830) to analyze the short-current photoresponse signals. We observed no drop in photoresponsivity within our experimental temporal resolution (up to 10 kHz). Both $V_{\rm DS}$ and $V_{\rm BG}$ were set to zero during the measurement.

To quantitatively investigate the capillary-force-assisted transfer method, we developed a transfer model basing on adhesion force analysis. In general, the adhesion force between two surfaces contains three types of force-van der Waals force, electrostatic force, and capillary force. The former two play critical roles in dry conditions but are dramatically weakened in a liquid (humid) environment due to the charge screening effect from the highly polarized water molecules.²⁷ To calculate the capillary force, we consider the model of a capillary meniscus at the touching region between a half PDMS cylinder and a flat surface, and a liquid bridge formed from the water sandwiched between the PDMS and substrate (Figure 5a,b). The capillary force is the result of both the surface tension around the circumference on the solid-liquid-gas interface and the Laplace pressure inside the liquid bridge. If the bending radius of PDMS (R) is much larger than the segment lengths of the liquid bridge $(s_1 \text{ and } s_2)$, the capillary adhesion force can be

$$F_{\text{cap}} = \frac{2\gamma_{\text{L}}(\cos\theta_1 + \cos\theta_2)}{\alpha} \tag{1}$$

where $\gamma_{\rm L}$ is the surface tension coefficient of the water—air interface (\sim 72.9 mN/m at 20 °C), θ_1 and θ_2 refer to the water contact angles on the PDMS film and the substrate, and α is the angle between the substrate and the outer tangent line of the PDMS at the meniscus edge. The detailed derivation of eq 1 is described in the Supporting Information. It is significant to note that the contact angle should be the dynamic dewetting contact angle (receding angle) instead of the static contact angle in this equation because the capillary bridge is sliding on

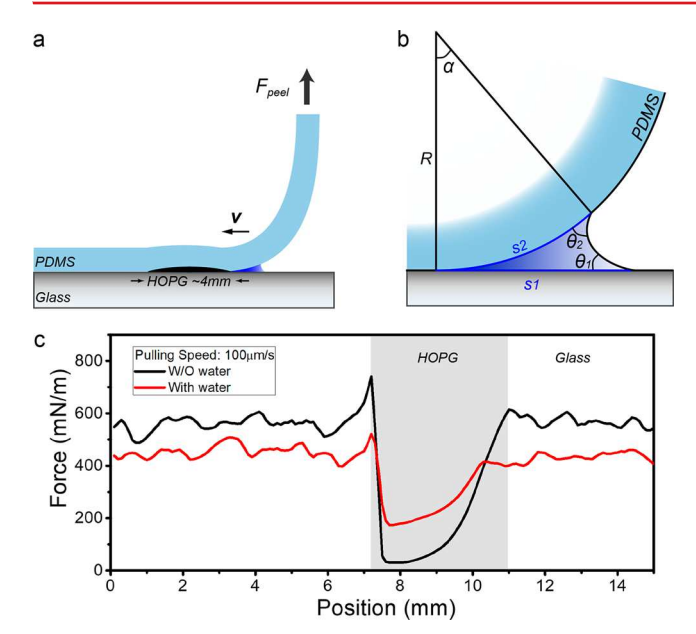


Figure 5. Capillary force model analysis and experimental measurement. (a) Schematic of the adhesion force measurement using a thin PDMS stripe stamp on the target substrate, which contains a 4 mm wide HOPG region. (b) Mechanism schematic of capillary interaction between PDMS and substrate. (c) Adhesion force measurement under dry and wet conditions, measured at a peeling-off rate of 100 μ m/s. The adhesion force on HOPG is dramatically increased under the presence of a meniscus bridge.

both the PDMS surface and the substrate during the peeling-off process. In general, the receding angle is much smaller than the static contact angle, which leads to a positive (attractive) capillary force in eq 1 for even hydrophobic substrates such as pristine PDMS (with a static contact angle of $\sim 110^{\circ}$). To evaluate the receding angles on different materials, we performed a tilted-plate measurement²⁸ by using a digital goniometer integrated with a syringe needle to record the droplet of deionized water placed on the surfaces of tilted substrates. Water drops on PDMS, glass, and highly oriented pyrolytic graphite (HOPG) substrates give receding angles of 50°, 23°, and 49°, respectively (Figure S5). Here, HOPG is used to mimic the graphene flake surface. We also measured the angle α by measuring the contact angle between a thin PDMS film (~2 mm in thickness) and the SiO₂ substrate with different peeling speeds and found it to be in the range of $5^{\circ}-30^{\circ}$. Using eq 1, we can estimate the capillary forces between PDMSwater-glass and PDMS-water-HOPG interfaces to be in the ranges of 0.45-2.6 N/m and 0.38-2.2 N/m, respectively.

To verify this capillary force model, we measured the adhesion force between a thin PDMS film and various substrates under dry and wet conditions. A laboratory-developed peeling-off apparatus is used to record the peeling-off force ($F_{\rm peel}$) needed to separate a PDMS strip from different substrates at velocity ν . As shown in Figure 5b, a typical specimen contains SiO₂ regions and a 4 mm wide HOPG region, which is formed of thin HOPG flakes flattened on the SiO₂ substrate. Before measuring the dry-condition $F_{\rm peel}$, the freshly prepared PDMS strips were placed on the substrate directly, followed by 1 h of relaxation to release stress. To measure the wet-condition $F_{\rm peel}$, the PDMS strip was hung over a beaker with boiling water for a few seconds to condense water and then placed on the sample substrate for the immediate

measurement. F_{peel} is measured at a low peeling-off rate of 100 μ m/s. Both the mechanical energy stored in the PDMS film²⁹ and the influence from the weight change in the vertical part of the PDMS strip were compensated in the data analysis. The black curve in Figure 5c shows the F_{peel} at the dry condition. It starts at around 550 mN/m on SiO₂ and drops steeply to ~40 mN/m when the separation region reaches the SiO₂-to-HOPG boundary. At the $\hat{H}OPG$ -to- $\hat{S}iO_2$ boundary, F_{peel} gradually returns to 550 mN/m. Next, the separation front starts to move on again, and F_{peel} remains at around 550 mN/m. Because the F_{peel} on glass stays at a similar level throughout the operation of the experiment (\sim 3 min), we believe that the swelling effect in PDMS, which is at the time scale of hours, 30 can be ignored here. The adhesion energy between HOPG and PDMS (~40 mJ/m²) is much lower than that between a graphene monolayer and SiO₂ (\sim 240 mJ/m²), which explains why PDMS cannot pick up a graphene monolayer directly from a SiO_2 substrate. In the wet-condition measurement, F_{peel} is lowered to ~450 mN/m on the SiO₂ surface, but on the HOPG surface, it significantly increases to ~200 mN/m. It is large enough to overcome the binding energy between graphene and SiO₂, leading to the peeling-off of graphene from the substrate. Moreover, the $F_{\rm peel}$ in our experiment is limited by the large surface roughness of HOPG flakes (more details are given in the Supporting Information), which increases the average a and lowers the $F_{\rm peel}$. The adhesion energy on a flat graphene surface can be larger than 200 mJ/m², which may be utilized to transfer 2D materials from more adhesive substrates, such as metals. We tested this transfer method on graphene monolayers and MoS2 monolayer domains prepared by chemical vapor deposition (CVD) methods on copper films and SiO₂ substrates, respectively. Because the adhesion energy between graphene and Cu surface is high (\sim 720 mJ/m²³¹), only about half of the total area was transferred (see Figure S7). In the CVD-MoS2 case, all of the MoS₂ domains were transferred (Figure S8).

In summary, a simple and clean stamp transfer method for 2D materials is developed. Using a thin layer of water as an instant yet temporary glue, the adhesion energy between PDMS and 2D materials can be significantly increased during the peeling off process and restored shortly to facilitate the releasing process. The Gr-FET device characterization reveals a very low impurity level on graphene monolayer after the transfer. High-quality Gr/MoS₂/Gr vertical heterostructures with clean interfaces are fabricated to show the convenience of this method for constructing complicated heterostructures. Moreover, the mechanism model study discloses that higher capillary force can be achieved by using smaller contact angle α between PDMS and the substrate, which will stimulate further investigation of using this method for transferring large-scale 2D materials and accelerate the development of 2D material studies.

Method. *PDMS Preparation.* A standard PDMS preparation recipe was used. In a clean plastic tube, PDMS and hardener were mixed at a ratio of 9:1 (Dow Corning, Sylgard 184). The noncloth end of a plastic swab was used to mix the solution for 5 min. Glass slides were cleaned with Piranha solution (98% $\rm H_2SO_4/30\%~H_2O_2=3:1$) for 1 h and rinsed with DI water for 2 min. The cleaned slides were placed in a Petri dish and the mixed PDMS solution poured on the slides until ~2 mm in thickness. A total of 1 h was allowed to pass to vent bubbles, and the material was baked at 50 °C for 10 h. The PDMS was cut into the desired sizes and cleaned in isopropyl

alcohol (IPA) and DI water sonication for 2 min each before use.

FET Electrode Preparation. The Si wafer (with 300 nm thermal oxide) was first cleaned with Piranha solution for 1 h, then rinsed with acetone, IPA, and DI water, respectively. Standard photolithography and e-beam evaporation were used to define the electrodes (10, 80, and 3 nm for Pd, Au, and Cr, respectively, from top to bottom). After lift-off in acetone, the substrates were cleaned in IPA and DI water sonication for 10 min each before use.

2D Material Transfer. The graphene and MoS_2 flakes were prepared using the standard mechanical exfoliation method on 300 nm SiO_2/Si substrates. A total of ~ 50 mL of DI water in a 100 mL beaker was preheated on a hot plate (Fisher Scientific, Isotemp) at 120 °C to generate stable steam. The cleaned PDMS piece was held over the steam for 3–5 s to condense water and then placed gently on the SiO_2/Si substrate. Note that long-term water condensing may lead to distorted transfer results. A period of a few seconds was given to relax the film and peel it off from one side. The 2D flakes attached to PDMS and were then ready to be released. The release was conducted under an optical microscope to locate the position of electrodes. A simple stamping procedure is sufficient to leave the 2D flakes to the substrate.

ASSOCIATED CONTENT

S Supporting Information

The Supporting Information is available free of charge on the ACS Publications website at DOI: 10.1021/acs.nano-lett.7b03449.

A video showing the transfer process. (AVI)

A video showing the role of water in capillary-force transfer. (AVI)

Additional information on comparison with the conventional transfer method, capillary force model and derivation, transfer results with other liquids, influence from liquid layer thickness to the transfer results, dynamic contact angle measurement, angle α measurement, the transfer of CVD graphene and MoS₂ results, HOPG flake characterization, FET analysis, the role of water in the transfer method, and the influence of flake thickness. (PDF)

AUTHOR INFORMATION

Corresponding Author

*E-mail: ming@ece.ucr.edu.

ORCID ®

Xuezhi Ma: 0000-0003-3607-1145 Ming Liu: 0000-0001-9849-1845

Notes

The authors declare no competing financial interest.

■ ACKNOWLEDGMENTS

This work is supported by NSF Grants CAREER DMR-1654746 and DMR-1649795. We thank Dr. Nathaniel Gabor for the use of optical microscope alignment setup.

■ REFERENCES

- (1) Huang, X.; Yin, Z. Y.; Wu, S. X.; Qi, X. Y.; He, Q. Y.; Zhang, Q. C.; Yan, Q. Y.; Boey, F.; Zhang, H. Small 2011, 7, 1876–1902.
- (2) Novoselov, K. S.; Fal'ko, V. I.; Colombo, L.; Gellert, P. R.; Schwab, M. G.; Kim, K. Nature **2012**, 490, 192–200.

- (3) Zhang, Y.; Zheng, B.; Zhu, C.; Zhang, X.; Tan, C.; Li, H.; Chen, B.; Yang, J.; Chen, J.; Huang, Y.; Wang, L.; Zhang, H. *Adv. Mater.* **2015**, 27, 935–939.
- (4) Toth, P. S.; Velický, M.; Bissett, M. A.; Slater, T. J. A.; Savjani, N.; Rabiu, A. K.; Rakowski, A. M.; Brent, J. R.; Haigh, S. J.; O'Brien, P.; Dryfe, R. A. W. *Adv. Mater.* **2016**, *28*, 8256–8264.
- (5) Shi, J. P.; Liu, M. X.; Wen, J. X.; Ren, X. B.; Zhou, X. B.; Ji, Q. Q.; Ma, D. L.; Zhang, Y.; Jin, C. H.; Chen, H. J.; Deng, S. Z.; Xu, N. S.; Liu, Z. F.; Zhang, Y. F. *Adv. Mater.* **2015**, *27*, 7086.
- (6) Li, Q.; Zhao, Z.; Yan, B.; Song, X.; Zhang, Z.; Li, J.; Wu, X.; Bian, Z.; Zou, X.; Zhang, Y.; Liu, Z. Adv. Mater. 2017, 29, 1701325.
- (7) Suk, J. W.; Kitt, A.; Magnuson, C. W.; Hao, Y. F.; Ahmed, S.; An, J. H.; Swan, A. K.; Goldberg, B. B.; Ruoff, R. S. *ACS Nano* **2011**, *5*, 6916–6924.
- (8) Liang, X. L.; Sperling, B. A.; Calizo, I.; Cheng, G. J.; Hacker, C. A.; Zhang, Q.; Obeng, Y.; Yan, K.; Peng, H. L.; Li, Q. L.; Zhu, X. X.; Yuan, H.; Walker, A. R. H.; Liu, Z. F.; Peng, L. M.; Richter, C. A. ACS Nano 2011, 5, 9144–9153.
- (9) Kidambi, P. R.; Boutilier, M. S. H.; Wang, L.; Jang, D.; Kim, J.; Karnik, R. *Adv. Mater.* **2017**, *29*, 1605896.
- (10) Desai, S. B.; Madhvapathy, S. R.; Amani, M.; Kiriya, D.; Hettick, M.; Tosun, M.; Zhou, Y. Z.; Dubey, M.; Ager, J. W.; Chrzan, D.; Javey, A. *Adv. Mater.* **2016**, *28*, 4053–4058.
- (11) Li, H.; Wu, J. M. T.; Huang, X.; Yin, Z. Y.; Liu, J. Q.; Zhang, H. ACS Nano **2014**, 8, 6563–6570.
- (12) Meitl, M. A.; Zhu, Z. T.; Kumar, V.; Lee, K. J.; Feng, X.; Huang, Y. Y.; Adesida, I.; Nuzzo, R. G.; Rogers, J. A. *Nat. Mater.* **2006**, *5*, 33–
- (13) Kim, K. S.; Zhao, Y.; Jang, H.; Lee, S. Y.; Kim, J. M.; Kim, K. S.; Ahn, J. H.; Kim, P.; Choi, J. Y.; Hong, B. H. *Nature* **2009**, 457, 706–710
- (14) Scharfenberg, S.; Rocklin, D. Z.; Chialvo, C.; Weaver, R. L.; Goldbart, P. M.; Mason, N. Appl. Phys. Lett. 2011, 98, 091908.
- (15) Boddeti, N. G.; Koenig, S. P.; Long, R.; Xiao, J. L.; Bunch, J. S.; Dunn, M. L. *J. Appl. Mech.* **2013**, *80*, 040909.
- (16) Pizzocchero, F.; Gammelgaard, L.; Jessen, B. S.; Caridad, J. M.; Wang, L.; Hone, J.; Boggild, P.; Booth, T. J. Nat. Commun. 2016, 7, 11804
- (17) Kim, K.; Yankowitz, M.; Fallahazad, B.; Kang, S.; Movva, H. C. P.; Huang, S. Q.; Larentis, S.; Corbet, C. M.; Taniguchi, T.; Watanabe, K.; Banerjee, S. K.; LeRoy, B. J.; Tutuc, E. *Nano Lett.* **2016**, *16*, 1989–1995.
- (18) Wang, L.; Meric, I.; Huang, P. Y.; Gao, Q.; Gao, Y.; Tran, H.; Taniguchi, T.; Watanabe, K.; Campos, L. M.; Muller, D. A.; Guo, J.; Kim, P.; Hone, J.; Shepard, K. L.; Dean, C. R. *Science* **2013**, 342, 614–617
- (19) Lock, E. H.; Baraket, M.; Laskoski, M.; Mulvaney, S. P.; Lee, W. K.; Sheehan, P. E.; Hines, D. R.; Robinson, J. T.; Tosado, J.; Fuhrer, M. S.; Hernandez, S. C.; Walton, S. G. *Nano Lett.* **2012**, *12*, 102–107.
- (20) Kim, H. H.; Kang, B.; Suk, J. W.; Li, N.; Kim, K. S.; Ruoff, R. S.; Lee, W. H.; Cho, K. ACS Nano **2015**, *9*, 4726–4733.
- (21) Nagpal, P.; Lindquist, N. C.; Oh, S. H.; Norris, D. J. Science **2009**, 325, 594–597.
- (22) Zhu, X. L.; Zhang, Y.; Zhang, J. S.; Xu, J.; Ma, Y.; Li, Z. Y.; Yu, D. P. Adv. Mater. 2010, 22, 4345.
- (23) Kim, S.; Nah, J.; Jo, I.; Shahrjerdi, D.; Colombo, L.; Yao, Z.; Tutuc, E.; Banerjee, S. K. *Appl. Phys. Lett.* **2009**, *94*, 062107.
- (24) Dean, C. R.; Young, A. F.; Meric, I.; Lee, C.; Wang, L.; Sorgenfrei, S.; Watanabe, K.; Taniguchi, T.; Kim, P.; Shepard, K. L.; Hone, J. *Nat. Nanotechnol.* **2010**, *5*, 722–726.
- (25) Britnell, L.; Gorbachev, R. V.; Jalil, R.; Belle, B. D.; Schedin, F.; Mishchenko, A.; Georgiou, T.; Katsnelson, M. I.; Eaves, L.; Morozov, S. V.; Peres, N. M. R.; Leist, J.; Geim, A. K.; Novoselov, K. S.; Ponomarenko, L. A. *Science* **2012**, *335*, 947–950.
- (26) Yu, W. J.; Liu, Y.; Zhou, H. L.; Yin, A. X.; Li, Z.; Huang, Y.; Duan, X. F. Nat. Nanotechnol. **2013**, *8*, 952–958.
- (27) Cadirov, N.; Booth, J. A.; Turner, K. L.; Israelachvili, J. N. ACS Appl. Mater. Interfaces 2017, 9, 14497—14505.

(28) Macdougall, G.; Ockrent, C. Proc. R. Soc. London, Ser. A 1942, 180, 151-173.

- (29) Nase, J.; Ramos, O.; Creton, C.; Lindner, A. Eur. Phys. J. E: Soft Matter Biol. Phys. **2013**, 36, 103.
- (30) Koh, K.-S.; Chin, J.; Chia, J.; Chiang, C.-L. Micromachines 2012, 3, 427–441.
- (31) Yoon, T.; Shin, W. C.; Kim, T. Y.; Mun, J. H.; Kim, T. S.; Cho, B. J. Nano Lett. **2012**, 12, 1448–1452.